RESEARCH LETTER

Upper crustal shear-wave velocity structure Beneath Western Java, Indonesia from seismic ambient noise tomography

Shindy Rosalia[1,2]* , Sri Widiyantoro[1,2,3], Phil R. Cummins[1,4], Tedi Yudistira[1], Andri Dian Nugraha[1,2], Zulfakriza Zulfakriza[1,2] and Ahmad Setiawan[5]

Abstract

This paper presents the depth inversion of Rayleigh wave group velocity to obtain an S-wave velocity model from seismic ambient noise cross-correlation in western Java, Indonesia. This study utilizes the vertical component data of a temporary seismograph network deployed in 2016, which was used in a previous study to estimate fundamental mode Rayleigh wave group velocity maps. In this study, the Neighborhood Algorithm was applied to invert the Rayleigh wave group velocities into 1D shear-wave velocity (*Vs*) profiles, which were then interpolated to produce a high-resolution, pseudo-3D *Vs* model. These tomographic images of *Vs* extend to ~ 20 km depth and show a pronounced NE-SW contrast of low and high *Vs* in the depth range 1–5 km that correlates well with the Bouguer anomaly map. We interpret the low *Vs* in the northeastern part of the study area as associated with alluvial and volcanic products from the Sunda Shelf and modern volcanic arc, whereas the high *Vs* in the southwestern part is associated with volcanic arc products from earlier episodes of subduction. We also obtained the depth of the northern Java Basin, which is in the range of 5–6 km, and the Garut Basin, which extends to 5 km depth. For greater depths, *Vs* gradually increases throughout western Java, which reflects the crystalline basement. This study provides estimates of the shallow crustal Vs structure underneath West Java with higher resolution than previous tomographic studies, which could be useful for supporting future earthquake studies in the region.

Keywords: Western Java, Ambient noise tomography, Crustal structure

Introduction

The island of Java, Indonesia, is part of the Sunda Arc, where the Australian Plate subducts in an almost arc-normal direction beneath the Sunda Block, on the southeastern margin of the Eurasian Plate, with a convergence rate that increases from 58 to 65 mm/year from west to east (Koulali et al. 2017). The western part of Java, the area of interest in this study, experiences seismicity due to this tectonic activity. Even though no megathrust

earthquakes greater than magnitude 8 are known to have occurred offshore Java, several recent subduction zone earthquakes have been large enough to cause damage and/or evacuation of buildings in western Java. These include the 17 July 2006 Mw 7.7 Pangandaran tsunami earthquake (Ammon et al. 2006; Fujii and Satake 2006), the 2 September 2009 Mw 7.0 south of Tasikmalaya earthquake (Suardi et al. 2014; Gunawan et al. 2019), the 15 December 2017 Mw 6.5 earthquake near Pangandaran (Sirait et al. 2020), the 23 January 2018 Mw 5.9 offshore Lebak, Banten area (Sirait et al. 2020), and the 2 August 2019 Mw 6.9 on the southern coast of Banten (Fig. 1). We list these events in Table 1.

Historically, large earthquakes on crustal faults in western Java have caused widespread damage (Griffin

*Correspondence: shindyrosalia@itb.ac.id
[1] Global Geophysics Research Group, Faculty of Mining and Petroleum Engineering, Institute of Technology Bandung, Jalan Ganesa No. 10, Bandung 40132, Indonesia
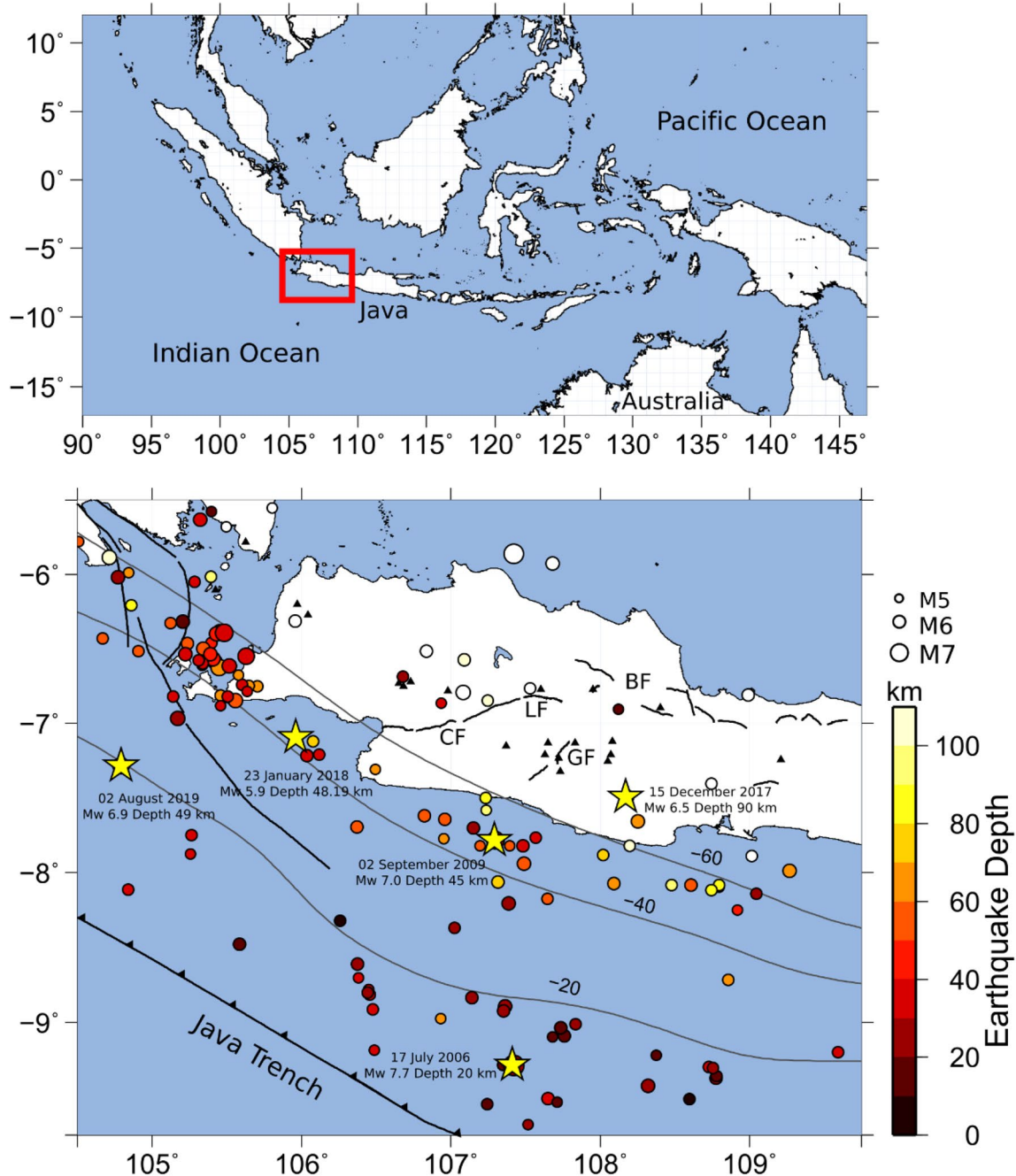Full list of author information is available at the end of the article

Fig. 1 Map showing the historical seismicity and major fault in the western part of Java. The colored circles show the seismicity from the USGS catalog for events with Mw ≥ 5.5 and the size of the circles represents the magnitude. The yellow star represents the major earthquakes in which the shaking could be felt in the major cities of West Java. The black lines denoted three major faults: Cimandiri Fault (CF), Lembang Fault (LF), Baribis Fault (BF), and Garsela Fault (GF). The fault is plotted from Pusat Studi Gempa Nasional (PuSGen) 2017 (see, Irsyam et al., 2020). Black triangles are active volcanoes, and gray lines are the slab2 contour (Hayes et al. 2018)

et al. 2019), and the possibility of great (Mw > 8) megathrust earthquakes with long return periods cannot be discounted (Widiyantoro et al. 2020). The potential for such earthquakes to cause much more extensive damage in major urban centers of western Java than have recent earthquakes is therefore of grave concern, especially in light of shallow basin structure that may enhance ground motion there (see Cipta et al. 2018a,

Table 1 Recent major earthquakes in the western part of Java

Date	Magnitude	Description	References
17 July 2006	Mw 7.7	Pangandaran Tsunami Earthquake with run up 5–8 m, ~ 800 killed and missing, MMI V	(Ammon et al. 2006; Fujii and Satake 2006)
2 September 2009	Mw 7.0	Tasikmalaya Earthquake with MMI VII in Tasikmalaya, ~ 110 killed, triggered landslide in Cikangkareng Area	(Suardi et al. 2014; Gunawan et al. 2019)
15 December 2017	Mw 6.5	Earthquake near Pangandaran with MMI maximum V-VI, many building damaged including hospital	(Sirait et al. 2020)
23 January 2018	Mw 5.9	Offshore Lebak, Banten Area. The shaking could be felt in a wide area (until Jakarta), many building damaged, 2 killed and 41 injuries	(Sirait et al. 2020)
2 August 2019	Mw 6.9	Labuan Earthquake, Southern coast of Banten. The shaking could be felt widely until Jakarta	USGS

b and Pranata et al., 2018, for Jakarta and Bandung, respectively).

Several studies have been conducted to obtain information on the western part of Java subsurface, including body wave tomography studies, e.g., a regional tomographic study using a double-difference method (Rosalia et al. 2019) and a non-linear tomographic study in eastern Sunda Arc using a combination of regional and global inversion (Widiyantoro et al. 2011). However, body wave tomography results have limited resolution at shallow depth, where there is not enough raypath coverage due to the earthquake source and station distribution.
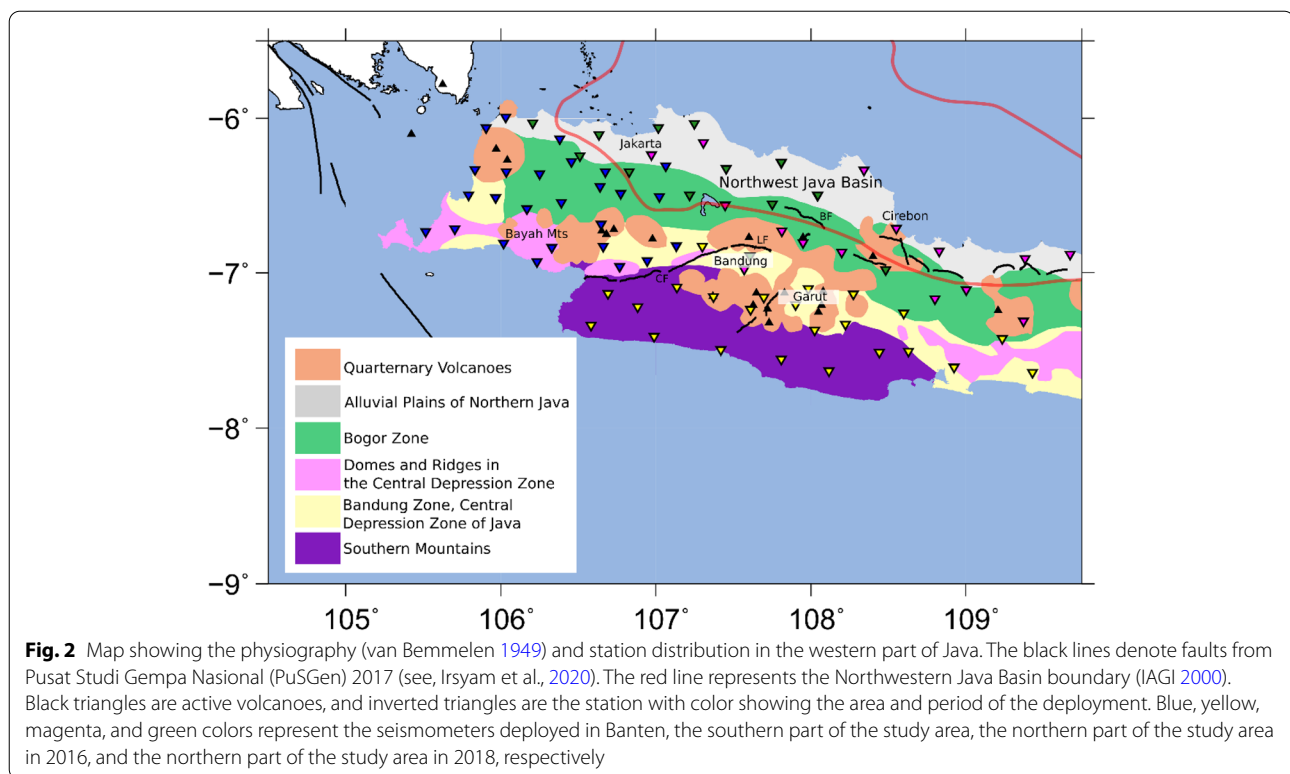
More detailed studies in some parts of western Java also have been conducted, e.g., in the Jakarta area using ambient noise tomography (Saygin et al. 2016), horizontal-to-vertical spectral ratio (HVSR) method (Cipta et al. 2018a), and microtremor array (Ridwan et al. 2017, 2019); in the Bandung area using ambient noise tomography (Pranata et al. 2020) and seismic microzonation using HVSR method (Pranata et al. 2018). A receiver function method was also applied in the western part of Java using a regional Meteorology, Climatology, and Geophysics Agency (BMKG) network, which gives a 1D velocity model beneath each station (Anggono et al. 2020). The study showed that crustal thickness varies between 25 and 32 km in the western part of Java. Even though some studies to obtain crustal structure information have been conducted in these limited areas, there is yet no Vs model that gives uniform coverage and resolves shallow crustal structure in western Java.

We applied the ambient noise tomography (ANT) method to obtain a regional shallow upper crustal S-wave velocity model beneath the western part of Java. In this study, we will focus on the depth inversion of Rayleigh wave group velocity maps from the previous study of Rosalia et al. (2020). From the inferred model, we will better understand the subsurface condition beneath the western part of Java. We also tried to obtain the

distribution of sedimentary deposits and in particular the depth of sedimentary basins in western Java.

Geological setting

The subduction margin of the western part of Java is at the transition between oblique subduction in Sumatra to nearly perpendicular subduction south of Java, with the subducting slab dipping at an angle of 60–65° beneath Java (Hamilton 1979; Malod et al. 1995; Widiyantoro and van der Hilst 1996). Based on physiography, van Bemmelen (1949) divided western Java into three EW trending zones: the coastal plain of Jakarta, the Bogor and Bandung zones, and the southern mountain zone (Fig. 2). Interspersed within the Bogor and Bandung Zones are domes, ridges, depressions, and Quaternary volcanoes. The Coastal Plain of Jakarta extends from west to east along the northern coast of western Java. This zone is part of the northern basinal area filled with Eocene–Oligocene non-marine clastic overlain by younger alluvial and volcanic deposits (van Bemmelen 1949; Bishop 2000). The Bogor Zone, which lies to the south of the Coastal Plain of Jakarta, consists of Miocene rock layers with igneous intrusions and hilly topography that extends to the west and east around the city of Bogor (van Bemmelen 1949; Martodjojo 1984; Satyana et al. 2002). The Bandung Zone consists of longitudinal tertiary ridges with depressions filled by volcanic deposits to form the plains of Sukabumi, Bandung, Garut, and Tasikmalaya (van Bemmelen 1949). The Southern Mountain Zone is a broad regional uplift in southern Java consisting of Paleogene volcanic arc rocks (van Bemmelen 1949; Soeria-Atmadja and Noeradi 2005; Hall et al. 2007). The quaternary volcanos of western Java are active andesitic volcanism mostly concentrated in the Bandung Zone (Mt. Tangkuban Perahu, Mt. Patuha, Mt. Guntur, Mt. Galunggung, and Mt. Papandayan). Basement rock underlying the sedimentary deposits in the western part of Java is exposed in the Ciletuh area, consists of serpentine metamorphic rocks with gabbro dykes,

Fig. 2 Map showing the physiography (van Bemmelen 1949) and station distribution in the western part of Java. The black lines denote faults from Pusat Studi Gempa Nasional (PuSGen) 2017 (see, Irsyam et al., 2020). The red line represents the Northwestern Java Basin boundary (IAGI 2000). Black triangles are active volcanoes, and inverted triangles are the station with color showing the area and period of the deployment. Blue, yellow, magenta, and green colors represent the seismometers deployed in Banten, the southern part of the study area, the northern part of the study area in 2016, and the northern part of the study area in 2018, respectively

pillow basalt, and volcanic breccia (van Bemmelen 1949; Parkinson et al. 1998; Hall et al. 2007; Clements et al. 2009).

Clements et al. (2009) interpreted an unconformity in the Ciletuh area as representing of a major thrusting event in the Late Miocene, in which the Southern Mountains were thrust onto the shelf sequences of the southern margin of the Sunda Block. Under this interpretation, the Southern Mountains are the remnant of a volcanic arc that formed in response to subduction of the Australian Plate in the Eocene and Early Miocene, resulting in the formation of a flexural basin between it and the margin of the Sunda Block to the north. After volcanic arc activity shifted northward to its present location, this Paleogene arc was thrust northward 50 km or more, over the basin, and onto the margin of the Sunda Block.

Data and methods

Ambient seismic noise has been widely used to study earth structure, using, e.g., ambient noise tomography (Yao et al. 2006; Lin et al. 2007; Gao et al. 2011; Saygin and Kennett 2012; Sammarco et al. 2017; Crowder et al. 2021) and the HVSR method (Gosar 2007; Cipta et al. 2018a, 2021; Harsuko et al. 2020). Ambient seismic noise used in ANT studies is usually generated by microseisms, resulting from the interaction between ocean waves and the solid earth (Snieder and Wapenaar 2010).

Microseisms generate ambient seismic noise at frequencies below 1 Hz, with the primary microseism energy, attributed to topographic coupling between ocean swell and seismic waves on the continental shelf, in the range 0.02–0.1 Hz, while secondary microseisms, attributed to non-linear forcing by ocean swell in both pelagic and coastal regions, are in the range 0.1–1 Hz (Nishida 2017). It has been shown that cross-correlating the ambient noise recorded simultaneously at a pair of seismographs can yield an estimate of the response of the medium (i.e., a point-source Green's function) that would be measured if there were a source at one of the two seismographs and a receiver at the other (Lobkis and Weaver 2001; Shapiro and Campillo 2004; Snieder and Wapenaar 2010).

Previous studies have shown that ANT can be used to image upper crustal seismic velocity structure in Indonesia, e.g., in Lake Toba (Stankiewicz et al. 2010), Ijen Volcano (Spica et al. 2015), Central Java (Zulfakriza et al. 2014), East Java (Martha et al. 2017), Tarutung pull-apart basin, Sumatra Fault (Ryberg et al. 2016), Banda Arc (Porritt et al. 2016), Jakarta (Saygin et al. 2016), Bandung Basin (Pranata et al. 2020), and Agung-Batur Volcano, Bali (Zulfakriza et al. 2020).

Rosalia et al. (2020) utilized a data set collected from 85 temporary broadband seismographic stations deployed in western Java during 2016–2018 (Fig. 2), to estimate interstation Green's functions using cross-correlations of

ambient seismic noise. They applied a trans-dimensional Bayesian approach to estimate fundamental mode Rayleigh wave group velocity maps from these data in the period range 1–25 s and showed how these maps correlate with surface geology and centers of volcanic activity. Here we consider the inversion of these 2D group velocity maps to estimate shear velocity (*Vs*) structure as a function of depth in the upper crust. We consider a grid of points regularly distributed throughout the study area, at which the Rayleigh wave group velocity maps define dispersion curves over the frequency range 0.04–1.00 Hz. Each Rayleigh wave group velocity dispersion curve is then inverted, resulting in a 1D Vs model with depth over 22 km at the respective grid point. The Vs depth profile at every grid points then interpolated to obtain a pseudo-3D model for Vs structure in the upper crust.

Depth inversion using neighborhood algorithm

We used the neighborhood algorithm (NA) to obtain *Vs* depth profiles at each point in a grid regularly distributed over the study area. The NA method is a Monte-Carlo global direct search method which uses successive sampling of the model space to assemble an ensemble of models that preferentially sample the low-misfit regions of the parameter space (Sambridge 1999a, b).

The NA utilizes a Voronoi cell tessellation in the model space in both a search and appraisal stage. The search stage consists of a direct search in multidimensional parameter space for an ensemble of models that preferentially sample its low-misfit region(s). In this stage, the NA first generates n_{s0} models randomly distributed throughout the model space. A mesh of Voronoi cells, each covering the nearest-neighbor portion of space associated with each model, is created. For each model, a theoretical dispersion curve is computed and the misfit between the theoretical and observation curve is assigned to the corresponding cell. Then, n_s new models are generated within each cell having lowest misfit. A new Voronoi cell tessellation is computed, new misfits are calculated, and the lowest-misfit cells are chosen to resample. This procedure is repeated, and the algorithm stops after a fixed number of iterations. The method results in fine sampling of portions of the model space associated with low misfit, while high-misfit regions are coarsely sampled. The appraisal stage consists of an algorithm for using the entire ensemble of models produced in the search stage to extract information about model uncertainty.

In this study, we produce a series of *Vs* depth profiles using the NA method to invert group velocity dispersion curves constructed from group velocity maps obtained using trans-dimensional tree inversion (Rosalia et al. 2020; Hawkins and Sambridge 2015). We grid the study area with intervals of latitude and longitude of 0.1°,

producing 557 grid points (Fig. 3a). In each point grid, a dispersion curve is extracted from the 2D group velocity maps at different periods. Each dispersion curve is then inverted using the Dinver package of Geopsy (Wathelet et al. 2004; Wathelet 2008) to generate a 1D shear-wave velocity profile at each corresponding grid point. The Dinver package uses a forward calculation of the dispersion curve based on the eigenvalue problem originally described by Thomson (1950) and Haskell (1953) and then modified by Dunkin (1965). The efficient root finding for the dispersion equation is achieved by utilizing Lagrange polynomials calculated using Neville's method (Press et al. 1992). After the theoretical dispersion curve has been calculated, the misfit value is evaluated using equation below (Wathelet et al. 2004):

$$
misfit = \sqrt{\sum_{i=0}^{n} \frac{(x_{di} - x_{mi})^2}{\sigma_i^2 n}}, \tag{1}
$$

where x_{di} is the velocity from the data curve at frequency f_i, x_{mi} is the velocity of the theoretical curve at frequency f_i, σ_i is the provided uncertainty estimate of the data curves, and *n* is the number of considered frequency samples. In this study, no uncertainty of data curves is provided. Based on Wathelet et al. (2004), σ_i is replaced by x_{di} if no uncertainty is provided. Combining all 1D *Vs* profiles from all grid points results in a 3D model of the subsurface.

In the NA, layered models are selected by choosing parameters from a specific range bounded by a priori minimum and maximum values. The layer parameters used in the surface wave inversion can be described using: S-wave velocity (Vs), thickness (H), P-wave velocity (Vp), and density (Wathelet et al. 2004; Wathelet 2008). The surface waves are less sensitive to Vp and density than to Vs (Takeuchi and Saito 1972; Bache et al. 1978; Tanimoto 1991; Aki and Richards 2002). Therefore, in this study we will just focus on *Vs* structure, by constraining Vp and density as descried below.

We parameterize our model based on the CRUST1.0 model (Laske et al. 2013). The CRUST1.0 model is specified on a 1° × 1° grid and incorporates global estimates of sediment thickness, which is used as guidance to determine the range of depth and velocity parameters. In this inversion, we used three horizontal layers and one half-space layer which is associated with one sediment, two crystalline crustal layers and a half-space, denoted Sediment and Crystalline Crust 1, 2, and 3, respectively, in Tables 2 and 3. Each layer is divided into sub-layers that are evenly spaced, with velocities determined by linear interpolation of the velocities at the top and bottom of the layer. The Sediment layer is divided into three sub-layers and the Crystalline Crust 1 and 2 layers are each
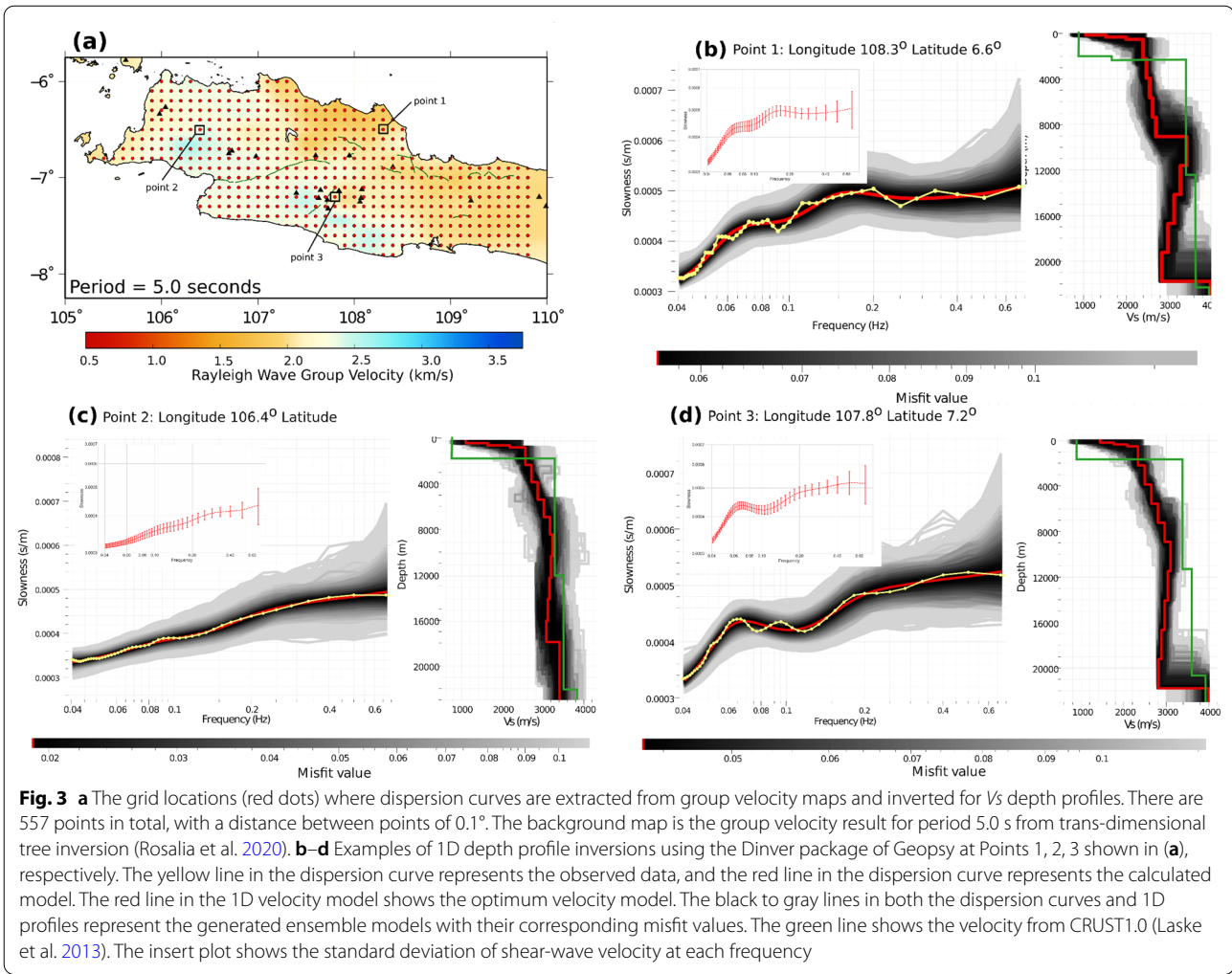
Rosalia *et al. Geoscience Letters*   (2022) 9:1

Page 6 of 14

Fig. 3 **a** The grid locations (red dots) where dispersion curves are extracted from group velocity maps and inverted for *Vs* depth profiles. There are 557 points in total, with a distance between points of 0.1°. The background map is the group velocity result for period 5.0 s from trans-dimensional tree inversion (Rosalia et al. 2020). **b–d** Examples of 1D depth profile inversions using the Dinver package of Geopsy at Points 1, 2, 3 shown in (**a**), respectively. The yellow line in the dispersion curve represents the observed data, and the red line in the dispersion curve represents the calculated model. The red line in the 1D velocity model shows the optimum velocity model. The black to gray lines in both the dispersion curves and 1D profiles represent the generated ensemble models with their corresponding misfit values. The green line shows the velocity from CRUST1.0 (Laske et al. 2013). The insert plot shows the standard deviation of shear-wave velocity at each frequency

Table 2 Model CRUST 1.0 (Laske et al., 2013) in the western part of Java

Layer	P-wave (km/s)	S-wave (km/s)	Density (g/cm^3)	Bottom Depth (km)
Sediment	2.0–3.6	0.6–1.9	1.9–2.3	1.39–4.30
Crystalline Crust 1	5.8–6.0	3.4–3.5	2.6–2.7	8.44–12.15
Crystalline Crust 2	6.3–6.6	3.6–3.8	2.7–2.9	20.56–21.92
Crystalline Crust 3	6.9–7.1	3.9–3.9	2.9–3.1	30–32

Table 3 The Range of Layer Parameters Used for *Vs* Inversion in Western Java

Layer	P-wave (km/s)	S-wave (km/s)	Density (g/cm^3)	Bottom depth (km)
Sediment	1.0–4.0	0.5–2.5	2.0	0.5–4.5
Crystalline Crust 1	3.0–8.0	2.0–3.5	2.1	5.00–11.5
Crystalline Crust 2	4.0–8.0	2.8–4.0	2.3	12.5–22.00
Crystalline Crust 3	6.0–8.0	3.0–4.0	2.6	Half-space

divided into five sub-layers. The inversion allows the top and bottom velocities and thickness of each layer to vary.

We noted the range of values for the layer parameters *Vp*, *Vs*, and depth taken on by the CRUST1.0 model in western Java (Table 2), but found these ranges were too narrow to be used as the range of layer parameters in our inversion. We therefore chose the wider bounds on layer parameters indicated in Table 3, in order to allow for the inversion to explore models that were outside the range of CRUST 1.0 model for western Java. In the inversion we assumed a fixed, uniform density in each layer of 2000 kg/m³, 2100 kg/m³, 2300 kg/m³, and 2700 kg/m³ for Sediment and Crystalline Crust 1, 2, and 3, respectively. In this inversion, the relation of *Vp* and *Vs* is constrained by allowing Poisson's ratio to vary from 0.2 to 0.5, which confines the search of parameter space to a physically reasonable range of elastic moduli.

Other parameters that should be considered are the two tuning parameters that control the behavior of the NA's exploitation (quick convergence of the misfit function) and exploration (investigation of nearly all local minima to find a global solution) of the model space. The parameters are the number of new models to sample at each iteration (n_s) and the number of resampled Voronoi cells (n_r). For the inversion parameters, we set the initial number of model samples (n_{s0}) initially before starting the iteration to 200, n_s to 100, and n_r to 100. Based on those parameterizations, we generate 50,200 models. In this inversion, we set the maximum number of iterations to 500.

Results and discussion

One-dimensional shear-wave profile

Results of inversion for selected 1D *Vs* profiles are shown in Fig. 3, with the location of each 1D *Vs* profile shown in Fig. 3a. Meanwhile, even though it has little sensitivity, the result of 1D *Vp* profiles is also shown in Fig. S1. Examples of dispersion curves and their associated Vs profiles are shown for Point 1 in the Banten area of westernmost Java, Point 2 in northern Java, and Point 3 in southern Java near the city of Garut (Fig. 3b–d, respectively). The misfit value at these points, as shown in Fig. 3, is less than 0.1, indicating that the calculated Vs model is close to the observed data. The best-fitting *Vs* models shown by the red curves are within the range of velocity for all models with misfit value < 0.2 (shown by grayscale curves in Fig. 3b–d). These estimated *Vs* profiles in Fig. 3b–d are compared with those of the CRUST1.0 model (green curves, from Laske et al, 2013). The standard deviation, as shown in the inset of Fig. 3, has a range of 0.05 to 0.2 km/s. In general, large standard deviation is observed in the high frequency of 0.6 Hz, which suggests that the shallower depth might not very well resolved.

The example of distribution of the ensemble models at depth 2, 5, 10, 15, and 20 km and its mean values are shown in Fig. S2.

CRUST1.0 includes an upper crustal sedimentary layer having $Vs = 0.88$ km/s that extends from the surface to 2 km depth throughout western Java. Our estimated *Vs* profiles also include a shallow, low-*Vs* layer, but *Vs* ranges from about 1 km/s at the surface to about 2.5 km/s at only 0.75 km depth. Hence, the gradient over the upper crustal sedimentary layer is much higher than that of CRUST1.0. Instead of the rapid jump at about 2.5 km depth to a $Vs > 3$ km/s that characterizes the transition from sedimentary to crystalline crustal layers in CRUST1.0, our estimated *Vs* profiles increase more gradually from 2.5 km/s at 0.75 km to higher velocities at mid-crustal depth. At Points 2 and 3 in the Banten and Garut areas, respectively, there appears to be a gradual increase to Vs > 3 km/s at about 9–10 km depth. In contrast, at Point 1 in the northern part of western Java, there is a weaker gradient in Vs from 0.75 to about 9 km depth, where there is a relatively sharp increase in velocity to > 3 km/s. Consequently, the average Vs in the uppermost 9 km of the crust is lower in the northeastern part of western Java than in the south or west.

Pseudo-3D *Vs* model

A pseudo-3D upper crustal *Vs* map was produced by interpolating the 1D profiles of the 557 grid points where dispersion curves were inverted. Plan views of the resulting *Vs* structure at selected depths between 0.5 and 18 km are shown in Fig. 4. The orange color corresponds to $Vs < 2.75$ km/s, which might be indicative of clastic rock of volcanic or sedimentary origin, while the blue color corresponds to $Vs > 2.75$ km/s and is indicative of a crystalline basement.

The *Vs* tomographic images in Fig. 4 reveal clear spatial patterns of high and low Vs anomalies that change with depth. At a depth of 0.5 km, all of western Java is characterized by low *Vs*, indicating the presence of quaternary sedimentary and volcanic deposits. At depth 1 to 5 km, we observed a regional pattern with a striking NE-SW contrast of low vs. high *Vs*. The northeastern half of western Java is characterized by low *Vs* with an average velocity of ~ 2.25 km/s. In contrast, the southwestern half is characterized by high *Vs* of ~ 2.75 km/s or higher. The tomographic result for depth 1–5 km correlates well with the Bouguer gravity anomaly map from the Geological Survey of Indonesia (PSG) shown in Fig. 5a. Based on the Bouguer anomaly map, the northeastern part of western Java, which is characterized by low *Vs*, exhibits a low Bouguer anomaly. The southwestern part of the western part of Java, characterized by high *Vs*, has a high Bouguer anomaly. The
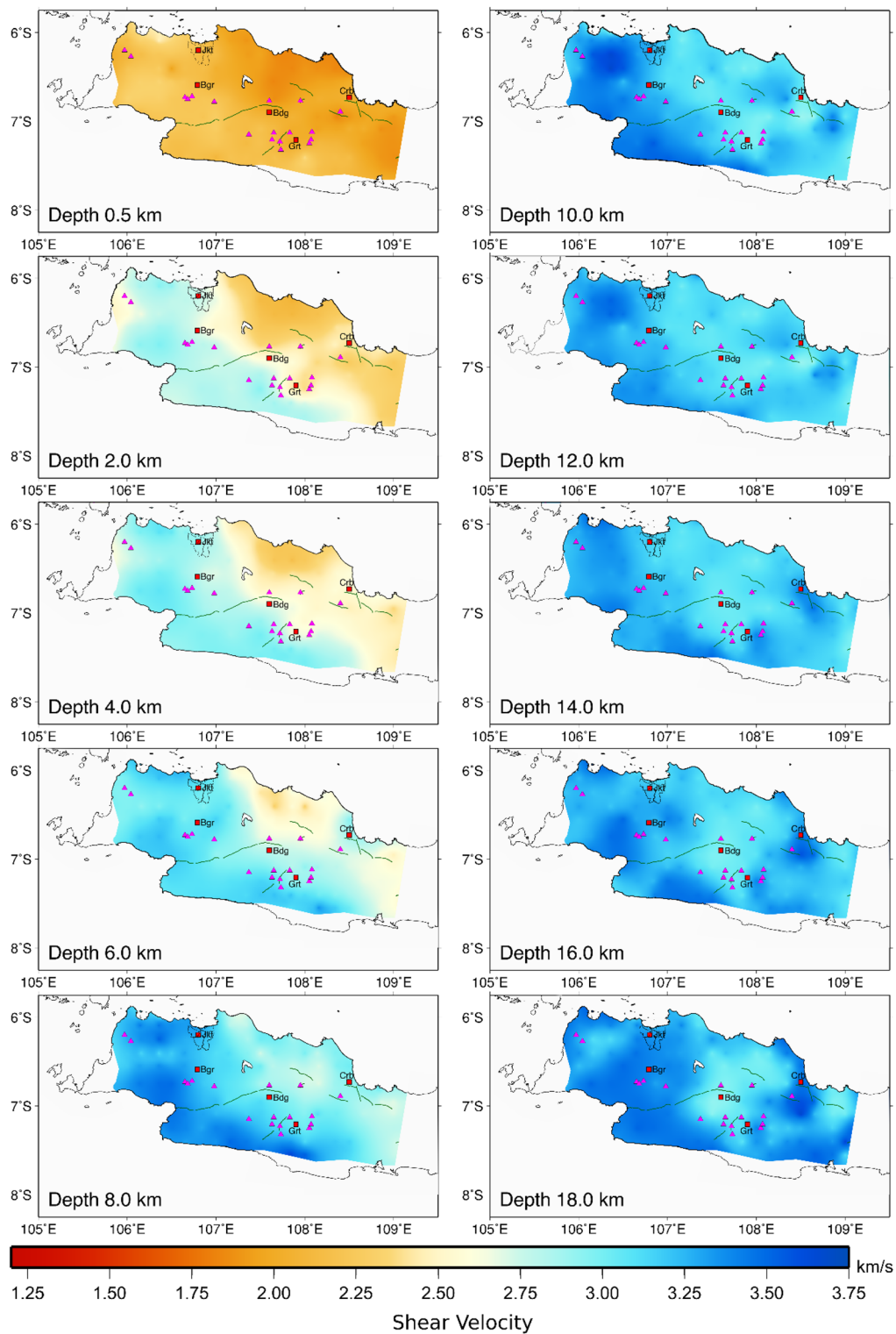
Fig. 4 The shear-wave velocity maps of the western part of Java from depth 0.5–18 km. The green curves are faults and the magenta triangles are volcanoes. The white colored areas are those with poor raypath coverage. Jkt, Bgr, Crb, Bdg, and Grt stand for the cities of Jakarta, Bogor, Cirebon, Bandung, and Garut, respectively
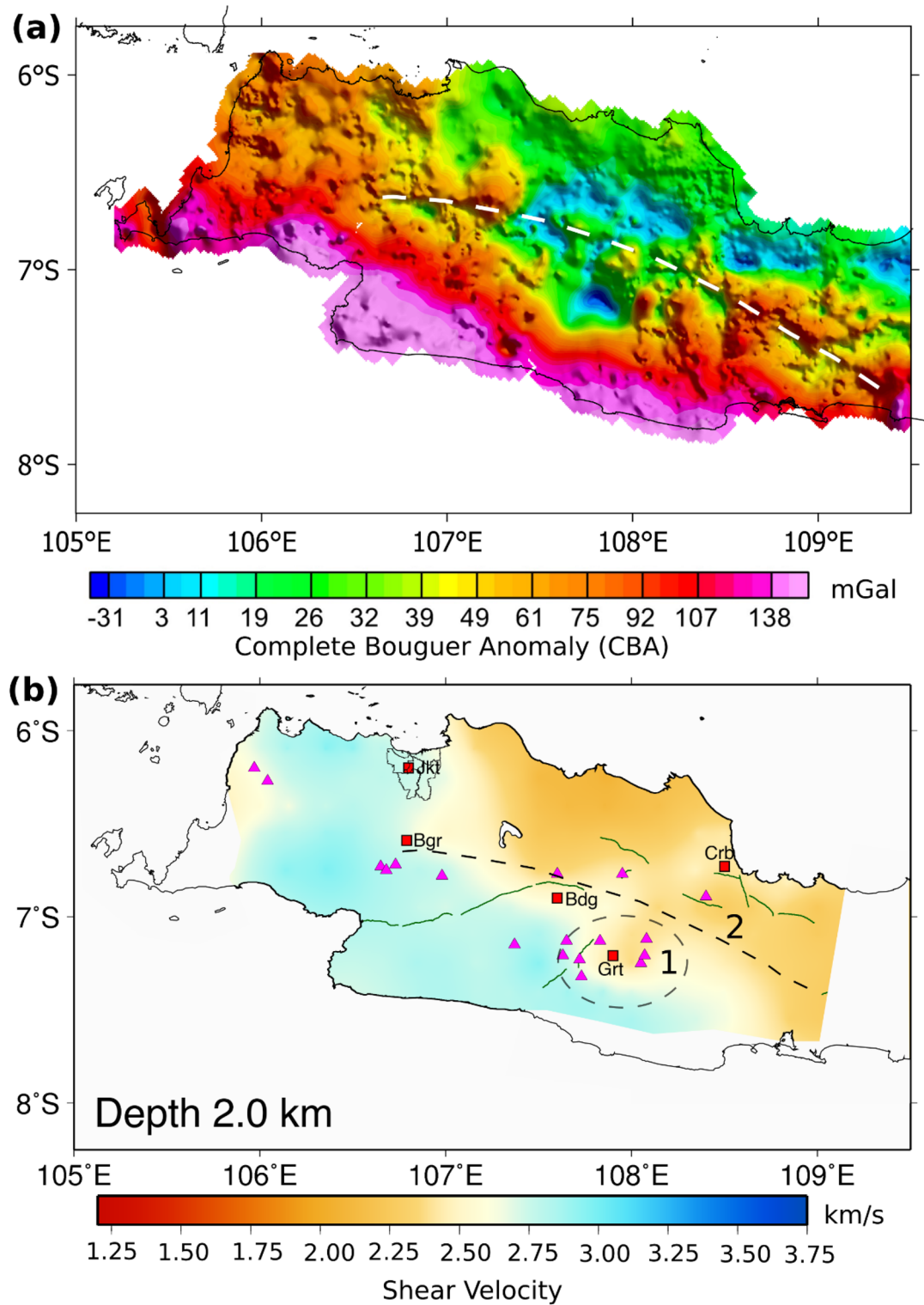
Fig. 5 **a** Complete Bouguer anomaly (CBA) map of western part of Java from Geological Survey of Indonesia (PSG). The white dashed line is the major structure delineated from the relief lineaments (Fauzi et al., 2015), **b** *Vs* maps from depth 2 km. Number 1 denotes the Garut Circular Feature and number 2 denotes the major structure line from CBA in **a**

boundary between these low and high *Vs* zones aligns remarkably well with the boundary between the low and high Bouguer anomaly (Fig. 5a vs. Fig. 5b).

The low *Vs* of 2.25 km/s in the depth range 1–5 km in the northeastern part of the study area, corresponding to the low Bouguer anomaly, is likely indicative of the same depositional products that fill the Northwest Java Basin that extends northward into the Java Sea: Eocene–Oligocene non-marine clastic, younger shallow shelf deposits, and late Tertiary and Quaternary volcanics (van Bemmelen 1949; Kingston 1988; Putra et al. 2016). A high *Vs* of 2.75 km/s over depths 1–5 km coincides with high Bouguer anomaly in the southern and western parts of the study area. The high *Vs* in the south underlies the Southern Mountain Zone, a broad regional uplift formed of Eocene and Miocene rocks of old andesite formation and the Ciletuh, Jampang, and Bayah formations (van Bemmelen 1949; Parkinson et al. 1998; Hall et al. 2007). Clements et al. (2009) showed that these are remnants of a submarine volcanic arc associated with subduction that began in the Eocene and were thrust northward by at least 50–100 km onto the southern edge of the Sunda Shelf. Because our ANT result and the Bouguer anomaly map show that both the high *Vs* and Bouguer gravity high extend much farther westward through all of the Banten area, we conjecture that this also reflects volcanic arc products of an earlier episode of subduction that now underlies all the westernmost part of Java, i.e., all of Banten as well as the Southern Mountains Zone.

The low velocity in the middle part of the study area is associated with depressions of the Bandung Zone, particularly the deep intermontane basins of Bandung and Garut, which are filled by coarse volcanoclastic, fluvial sediments, and a thick series of lacustrine deposits (van Bemmelen 1949; Dam et al. 1996). Low *Vs* in the Bandung Area was also found in the previous ANT study of Pranata et al. (2020), and interpreted to be associated with thick volcanoclastic deposits from Mt. Tangkuban Perahu and its massive predecessor, Mt. Sunda (see, Kartadinata et al. 2002; Nasution et al. 2004).

The Garut area, shown as a black dashed circle in (Fig. 5b), is associated with a low-*Vs* zone extending to at least 4 km depth, and is also in good agreement with the low Bouguer anomaly shown in Fig. 5a. We suggest that the low *Vs* might be associated with two subsurface conditions. First, the Garut Basin is thought to have formed as a pull-apart basin, with extension creating a deep basin that is now filled with sediments and pyroclastic deposits. Second, two major active volcanoes, Mt. Guntur and Mt. Papandayan, on the margin of the basin as well as geothermal activity show that there is abundant heat transfer and suggests the presence of deep and extensive hydrothermal and magmatic fluid systems (Fauzi et al.

2015). Both of these can account for the low *Vs* anomaly that extends to 5 km depth in the Garut area.

For depths ≥ 6 km, *Vs* gradually increases throughout western Java, especially in the Banten area and the southern mountain zone, which we surmise corresponds to the pre-tertiary metamorphic basement (van Bemmelen 1949; Hall et al. 2007; Clements et al. 2009; Putra et al. 2016). We also observed that *Vs* in this depth range beneath the active volcanoes in the Bandung and Garut areas is lower relative to its surroundings (Fig. 4). We suggest that the relatively low *Vs* might include a signature of volcanic activity, such as high temperature and/or partial melt.

Sedimentary basin geometry

Thick sedimentary basin fill, characterized by low *Vs* and low Bouguer anomaly, is observed in the northern and central part of the study area. The northern part is associated with the Northwest Java Basin; meanwhile, the center area is associated with the depressions in the Bandung Zone, particularly the Garut Basin. We show a perspective view of vertical cross sections in western Java in Fig. 6, to illustrate the depth and the geometry of these basins. The vertical cross section is passing through the northern Java plain, Bandung, and Garut Basin. Figure 6 shows that the deepest sedimentary basin is in the northern area, in the onshore part of the Northwest Java Basin, which contains several depocenters dominantly filled with a Tertiary sequence with thickness in excess of 5.5 km. Based on our cross section, the northern basin has a depth of ~ 5–6 km, and we observed the basin is still thickening to the north, to the center of the Northwest Java Basin. In Fig. 6, we also observed a bowl-like feature beneath Garut, which we suggest is associated with Garut Basin with depth up to ~ 5 km. There is a limited data to constraint the results using bore holes and active source data, especially in the southern and western part of study area. Based on a study of Putra et al. (2016) that shows a digital terrain model of the northern basin, the basement in this area ranges from ~ 3000 to 4000 km depth. Meanwhile, a geologic cross section of Arjuna Subbasin from Kingston (1988) shows that the basin thickness can reach 8000 km. For the Garut Basin area, the data is more limited, and we could not find any estimate of the basin depth in the literature, so we can only surmise the subsurface information from the Bouguer gravity anomaly data.

Conclusion

We successfully inverted ambient noise data to obtain a 3D shear-wave velocity model of the upper crustal structure beneath the western part of Java at higher resolution than has been obtained from any previous study. From
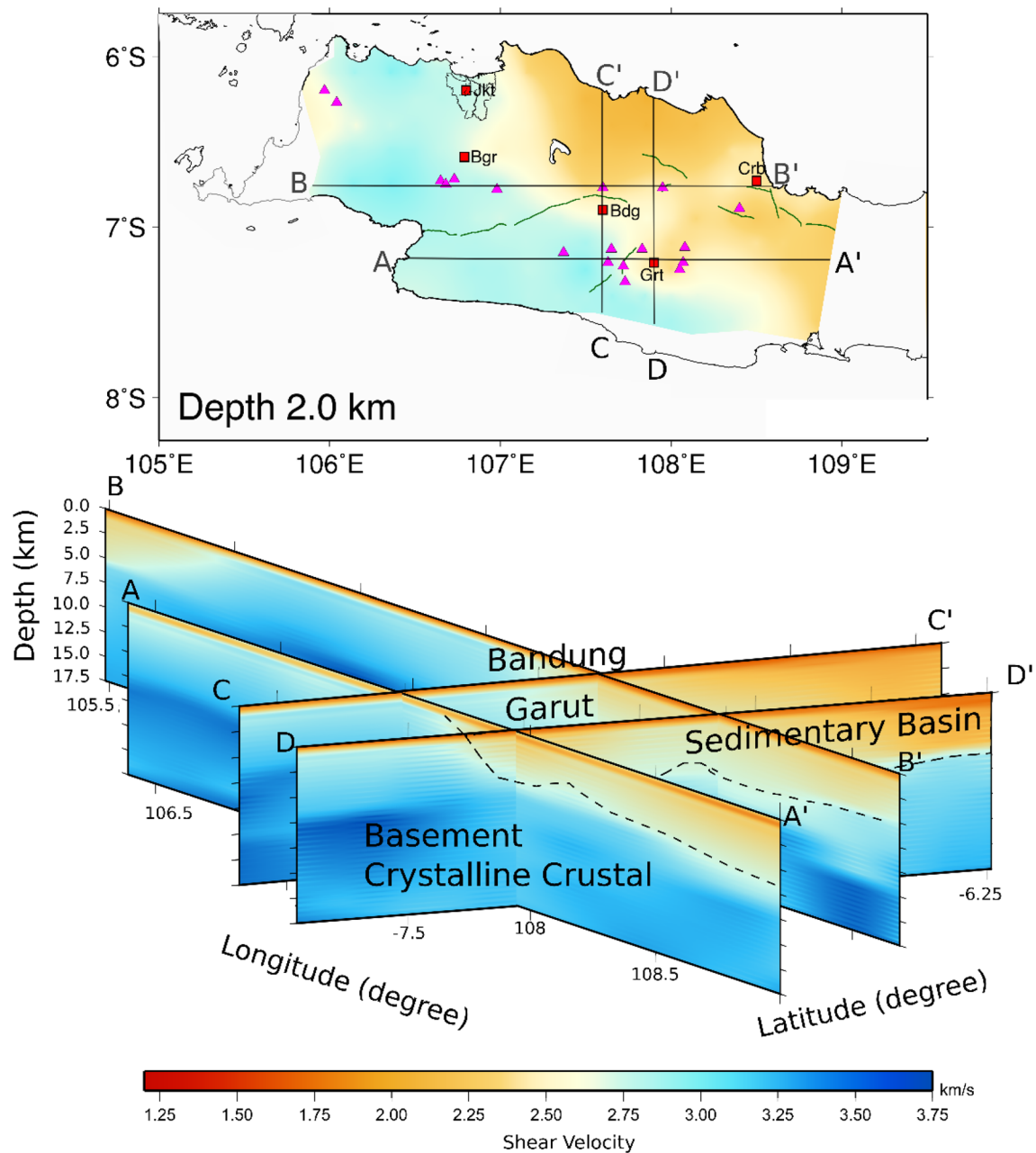
Fig. 6 Cross section of *Vs* model beneath the western part of Java. The low velocity associated with sedimentary deposit in the northern, Bandung, and Garut Basin, as well as the high velocity associated with the metamorphic and igneous crystalline crust are clearly evident

the Vs maps, we observe a NE-SW contrast of low and high Vs from the depth of 1–5 km, which aligns with low and high anomalies in the Bouguer anomaly map. The low Vs in the northern and central parts (Bandung and Garut Basin) of the study area is associated with basin fill consisting of Eocene–Oligocene non-marine clastic deposits, products of late Tertiary and Quaternary volcanism, and late Quaternary fluvial and lacustrine sediments. The depth of the northern basin is in a range of 5–7 km, while the depth of the Garut Basin is up to 5 km. At greater depths ≥ 6 km, Vs gradually increases throughout western Java, which reflects the crystalline crustal basement underlying this area.

Western Java includes several large population centers, including one of the world's largest urban agglomerations around Jakarta as well as the major cities of

Rosalia *et al. Geoscience Letters*   (2022) 9:1

Page 12 of 14

Bandung and Garut, all of which are located in sedimentary basins. While no major earthquakes have struck western Java since earthquake recording began in the early 20th Century, Griffin et al. (2019) and Nguyen et al. (2015) described several historical earthquakes in western Java that caused widespread destruction: an intraslab earthquake on 5 January 1699 near the Jakarta area with Mw ~ 7.5, and crustal earthquakes in 1780, 1834, and 1847. Were any of these earthquakes to recur today, they are all but certain to cause heavy damage in these urban population centers, not only because of the high population density but also due to basin resonance and amplification of seismic waves. The large-scale basin structure elucidated here is a first step toward understanding how important these effects may be, and when combined with more detailed models of basin structure may provide the basis for forecasting earthquake ground motion (see, e.g., Cipta et al., 2018b).

Supplementary Information

The online version contains supplementary material available at https://doi.org/10.1186/s40562-021-00208-5.

Additional file 1: Figure S1. A–c) Examples of 1D P-wave velocity profile inverted using dinver package of Geopsy at points 1, 2, 3 shown in Figure 3, respectively. The red line in the 1D velocity model shows the optimum velocity model. The black to gray lines represent the generated ensemble models with their corresponding misfit values. **Figure S2.** The distribution of the ensemble models generated at point 3 (longitude 107.8° and latitude 7.2°) at depth 2–20 km. The red dashed line is the mean value of the ensemble.

Availability of data and materials
The data that support the findings of this study are available from the corresponding author, S. Rosalia, upon request.

Declarations

Competing interests
The authors declare that they have no known competing financial interests or personal relationships that could have appeared to influenced the work reported in this paper.

Author details
[1] Global Geophysics Research Group, Faculty of Mining and Petroleum Engineering, Institute of Technology Bandung, Jalan Ganesa No. 10, Bandung 40132, Indonesia. [2] Center for Earthquake Science and Technology (CEST), Research Center for Disaster Mitigation, Institut Teknologi Bandung, Bandung 40132, Indonesia. [3] Faculty of Engineering, Maranatha Christian University, Bandung 40164, Indonesia. [4] Research School of Earth Sciences, Australian National University, Canberra, ACT 2601, Australia. [5] Geological Survey of Indonesia (PSG), Bandung 40122, Indonesia.

References
Aki K, Richards PG (2002) Quantitative Seismology, 2nd edn. W. H. Freeman and Co., San Francisco

Ammon CJ, Kanamori H, Lay T, Velasco AA (2006) The 17 July 2006 Java tsunami earthquake. Geophys Res Lett 33:1–5. https://doi.org/10.1029/2006GL028005

Anggono T, Syuhada S, Febriani F et al (2020) Crustal shear-wave velocity structure in Western Java, Indonesia from analysis of teleseismic receiver functions. J Earth Syst Sci. https://doi.org/10.1007/s12040-019-1288-1

Bache TC, Rodi WL, Harkrider DG (1978) Crustal structures inferred from Rayleigh-wave signatures of NTS explosions. Bull Seismol Soc Am 68:1399–1413

van Bemmelen RW (1949) The geology of Indonesia. 1, A. General geology of Indonesia and adjacent archipelagoes. US Government Printing Office

Bishop MG (2000) Petroleum systems of the Northwest Java Province, Java and offshore Southeast Sumatra, Indonesia

Cipta A, Cummins P, Dettmer J et al (2018a) Seismic velocity structure of the Jakarta Basin, Indonesia, using trans-dimensional Bayesian inversion of horizontal-to-vertical spectral ratios. Geophys J Int 215:431–449. https://doi.org/10.1093/gji/ggy289

Cipta A, Cummins P, Irsyam M, Hidayati S (2018b) Basin resonance and seismic hazard in jakarta, Indonesia. Geosci 8:1–25. https://doi.org/10.3390/geosciences8040128

Cipta A, Rudyanto A, Afif H et al (2021) Unearthing the buried Palu-Koro Fault and the pattern of damage caused by the 2018 Sulawesi Earthquake using HVSR inversion. Geol Soc London Spec Publ. https://doi.org/10.1144/sp501-2019-70

Clements B, Hall R, Smyth HR, Cottam MA (2009) Thrusting of a volcanic arc: a new structural model for Java. Pet Geosci 15:159–174. https://doi.org/10.1144/1354-079309-831

Crowder E, Rawlinson N, Cornwell DG et al (2021) New insights into North Sea deep crustal structure and extension from transdimensional ambient noise tomography. Geophys J Int 224:1197–1210. https://doi.org/10.1093/gji/ggaa475

Dam MAC, Suparan P, Nossin JJ et al (1996) A chronology for geomorphological developments in the greater Bandung area, West-Java, Indonesia. J Southeast Asian Earth Sci 14:101–115. https://doi.org/10.1016/S0743-9547(96)00069-4

Dunkin JW (1965) Computation of modal solutions in layered, elastic media at high frequencies. Bull Seismol Soc Am 55:335–358. https://doi.org/10.1785/BSSA0550020335

Fauzi A, Permana H, Indarto S, Gaffar EZ (2015) Regional Structure Control on Geothermal Systems in West Java, Indonesia

Fujii Y, Satake K (2006) Source of the July 2006 West Java tsunami estimated from tide gauge records. Geophys Res Lett 33:2–6. https://doi.org/10.1029/2006GL028049

Gao H, Humphreys ED, Yao H, van der Hilst RD (2011) Crust and lithosphere structure of the northwestern U.S. with ambient noise tomography: terrane accretion and Cascade arc development. Earth Planet Sci Lett 304:202–211. https://doi.org/10.1016/j.epsl.2011.01.033

Gosar A (2007) Microtremor HVSR study for assessing site effects in the Bovec basin (NW Slovenia) related to 1998 Mw5.6 and 2004 Mw5.2 earthquakes. Eng Geol 91:178–193. https://doi.org/10.1016/j.enggeo.2007.01.008

Griffin J, Nguyen N, Cummins P, Cipta A (2019) Historical earthquakes of the eastern sunda arc: source mechanisms and intensity-based testing of

Indonesia's national seismic hazard assessment. Bull Seismol Soc Am 109:43–65. https://doi.org/10.1785/0120180085

Gunawan E, Widiyantoro S, Marliyani GI et al (2019) Fault source of the 2 September 2009 Mw 6.8 Tasikmalaya intraslab earthquake, Indonesia: analysis from GPS data inversion, tsunami height simulation, and stress transfer. Phys Earth Planet Inter 291:54–61. https://doi.org/10.1016/j.pepi.2019.04.004

Hall R, Clements B, Smyth HR, Cottam MA (2007) A new interpretation of java's structure

Hamilton WB (1979) Tectonics of the Indonesian region

Harsuko MRC, Zulfakriza Z, Nugraha AD et al (2020) Investigation of Hilbert-Huang Transform and Fourier Transform for Horizontal-to-Vertical Spectral Ratio Analysis: Understanding the Shallow Structure in Mataram City, Lombok. Indonesia Front Earth Sci 8:334. https://doi.org/10.3389/feart.2020.00334

Haskell NA (1953) The dispersion of surface waves in multi-layered media. Bull Seism Soc Am 43:17–43

Hayes GP, Moore GL, Portner DE et al (2018) Slab2, a comprehensive subduction zone geometry model. Science (80-) 362:58–61. https://doi.org/10.1126/science.aat4723

Hawkins R, Sambridge M (2015) Geophysical imaging using trans-dimensional trees. Geophysical J Int 203(2):972–1000. https://doi.org/10.1093/gji/ggv326

IAGI IA of G (2000) An outline of the geology of Indonesia. Lereng Nusantara

Irsyam M, Cummins PR, Asrurifak M et al (2020) Development of the 2017 national seismic hazard maps of Indonesia. Earthq Spectra 36:112–136. https://doi.org/10.1177/8755293020951206

Kartadinata MN, Okuno M, Nakamura T, Kobayashi T (2002) Eruptive History of Tangkuban Perahu Volcano, West Java. Indonesia 地學雜誌 111:404–409. https://doi.org/10.5026/jgeography.111.3_404

Kingston J (1988) Undiscovered petroleum resources of Indonesia

Koulali A, McClusky S, Susilo S et al (2017) The kinematics of crustal deformation in Java from GPS observations: Implications for fault slip partitioning. Earth Planet Sci Lett 458:69–79. https://doi.org/10.1016/j.epsl.2016.10.039

Laske G, Masters G, Ma Z, Pasyanos M (2013) Update on CRUST1. 0—A 1-degree global model of Earth's crust. In: Geophys. Res. Abstr. p 2658

Lin F–C, Ritzwoller MH, Townend J et al (2007) Ambient noise Rayleigh wave tomography of New Zealand. Geophys J Int 170:649–666. https://doi.org/10.1111/j.1365-246X.2007.03414.x

Lobkis OI, Weaver RL (2001) On the emergence of the Green's function in the correlations of a diffuse field. J Acoust Soc Am 110:3011–3017. https://doi.org/10.1121/1.1417528

Malod JA, Karta K, Beslier MO, Zen MT (1995) From normal to oblique subduction: tectonic relationships between Java and Sumatra. J Southeast Asian Earth Sci 12:85–93. https://doi.org/10.1016/0743-9547(95)00023-2

Martodjojo S (1984) Evolution of Bogor Basin, West Java. Dr Thesis, Inst Teknol Bandung

Martha AA, Cummins P, Saygin E, et al (2017) Imaging of upper crustal structure beneath East Java–Bali, Indonesia with ambient noise tomography. Geosci Lett. https://doi.org/10.1186/s40562-017-0080-9

Nasution A, Kartabinata MN, Sutamingsih E et al (2004) Geology, age dating and geochemistry of the Tangkuban Parahu Geothermal Area, West Java, Indonesia. J Geotherm Res Soc Japan 26:285–303. https://doi.org/10.11367/grsj1979.26.285

Nguyen N, Griffin J, Cipta A, Cummins P (2015) Indonesia's historical earthquakes modelled examples for improving the national hazard map. Geosci Australia. https://doi.org/10.11636/record.2015.023

Nishida K (2017) Ambient seismic wave field. Proc Japan Acad Ser B Phys Biol Sci 93:423–448

Parkinson CD, Miyazaki K, Wakita K et al (1998) An overview and tectonic synthesis of the pre-Tertiary very-high-pressure metamorphic and associated rocks of Java, Sulawesi and Kalimantan, Indonesia. Isl Arc 7:184–200. https://doi.org/10.1046/j.1440-1738.1998.00184.x

Pranata B, Yudistira T, Saygin E et al (2018) Seismic microzonation of Bandung basin from microtremor horizontal-to-vertical spectral ratios (HVSR). AIP Conf Proc. https://doi.org/10.1063/1.5047289

Pranata B, Yudistira T, Widiyantoro S et al (2020) Shear wave velocity structure beneath Bandung basin, West Java, Indonesia from ambient noise tomography. Geophys J Int 220:1045–1054. https://doi.org/10.1093/gji/ggz493

Press WH, Teukolsky SA, Flannery BP, Vetterling WT (1992) Numerical recipes in Fortran 77: volume 1, volume 1 of Fortran numerical recipes: the art of scientific computing. Cambridge university press

Porritt RW, Miller MS, O'Driscoll LJ et al (2016) Continent–arc collision in the Banda Arc imaged by ambient noise tomography. Earth Planet Sci Lett 449:246–258. https://doi.org/10.1016/j.epsl.2016.06.011

Putra SDH, Suryantini SW (2016) Thermal modeling and heat flow density interpretation of the onshore Northwest Java Basin, Indonesia. Geotherm Energy. https://doi.org/10.1186/s40517-016-0052-x

Ridwan M, Widiyantoro S, Irsyam M et al (2017) Development of an engineering bedrock map beneath Jakarta based on microtremor array measurements. Geol Soc Spec Publ 441:153–165. https://doi.org/10.1144/SP441.7

Ridwan M, Cummins PR, Widiyantoro S, Irsyam M (2019) Site characterization using microtremor array and seismic hazard assessment for Jakarta, Indonesia. Bull Seismol Soc Am 109:2644–2657. https://doi.org/10.1785/0120190040

Rosalia S, Widiyantoro S, Dian Nugraha A et al (2019) Double-difference tomography of P- and S-wave velocity structure beneath the western part of Java, Indonesia. Earthq Sci 32:12–25. https://doi.org/10.29382/eqs-2019-0012-2

Rosalia S, Cummins P, Widiyantoro S et al (2020) Group velocity maps using subspace and transdimensional inversions: Ambient noise tomography in the western part of Java, Indonesia. Geophys J Int 220:1260–1274. https://doi.org/10.1093/gji/ggz498

Ryberg T, Muksin U, Bauer K (2016) Ambient seismic noise tomography reveals a hidden caldera and its relation to the Tarutung pull-apart basin at the Sumatran Fault Zone, Indonesia. J Volcanol Geotherm Res 321:73–84. https://doi.org/10.1016/j.jvolgeores.2016.04.035

Sambridge M (1999a) Geophysical inversion with a neighbourhood algorithm—I. Searching a parameter space. Geophys J Int 138:479–494. https://doi.org/10.1046/j.1365-246X.1999.00876.x

Sambridge M (1999b) Geophysical inversion with a neighbourhood algorithm: II. Appraising the Ensemble. Geophys J Int 138:727–746. https://doi.org/10.1046/j.1365-246x.1999.00900.x

Sammarco C, Cornwell DG, Rawlinson N (2017) Ambient noise tomography reveals basalt and sub-basalt velocity structure beneath the Faroe Islands, North Atlantic. Tectonophysics 721:1–11

Satyana AH, Armandita C, Raharjo B, Syafri I (2002) New observations on the Evolution of the Bogor Basin, West Java: opportunities for Turbidite Hydrocarbon Play. Bul Geol Inst Teknol BANDUNG—Ed KHUSUS 42 Tahun Pengabdi Prof Dr Soejono Martodjojo. Msc Dep Tek Geol FIKTM, ITB, Bandung 2002:1–16

Saygin E, Kennett BLN (2012) Crustal structure of Australia from ambient seismic noise tomography. J Geophys Res Solid Earth. https://doi.org/10.1029/2011JB008403

Saygin E, Cummins PR, Cipta A et al (2016) Imaging architecture of the Jakarta Basin, Indonesia with transdimensional inversion of seismic noise. Geophys J Int 204:918–931. https://doi.org/10.1093/gji/ggv466

Shapiro NM, Campillo M (2004) Emergence of broadband Rayleigh waves from correlations of the ambient seismic noise. Geophys Res Lett. https://doi.org/10.1029/2004GL019491

Sirait AMM, Meltzer AS, Waldhauser F et al (2020) Analysis of the 15 December 2017 Mw 6.5 and the 23 January 2018 Mw 5.9 Java Earthquakes. Bull Seismol Soc Am. https://doi.org/10.1785/0120200046

Snieder R, Wapenaar K (2010) Imaging with ambient noise. Phys Today 63:44–49. https://doi.org/10.1063/1.3490500

Soeria-Atmadja R, Noeradi D (2005) Distribution of early tertiary volcanic rocks in south Sumatra and west Java. Isl Arc 14:679–686. https://doi.org/10.1111/j.1440-1738.2005.00476.x

Spica Z, Caudron C, Perton M et al (2015) Velocity models and site effects at Kawah Ijen volcano and Ijen caldera (Indonesia) determined from ambient noise cross-correlations and directional energy density spectral ratios. J Volcanol Geotherm Res 302:173–189. https://doi.org/10.1016/j.jvolgeores.2015.06.016

Stankiewicz J, Ryberg T, Haberland C et al (2010) Lake Toba volcano magma chamber imaged by ambient seismic noise tomography. Geophys Res Lett 37:3–7. https://doi.org/10.1029/2010GL044211

Suardi I, Afnimar S, Yagi Y et al (2014) Moment tensor analysis of the September 2, 2009 Tasikmalaya, West Java earthquake using the waveform inversion method of near field data. Int J Tomogr Simul 63–74

Takeuchi H, Saito M (1972) Seismic surface waves. Methods Comput Phys 11:217–295

Tanimoto T (1991) Waveform inversion for three-dimensional density and S wave structure. J Geophys Res Solid Earth 96:8167–8189. https://doi.org/10.1029/91JB00196

Thomson WT (1950) Transmission of elastic waves through a stratified solid medium. J Appl Phys 21:89–93

Wathelet M (2008) An improved neighborhood algorithm: parameter conditions and dynamic scaling. Geophys Res Lett. https://doi.org/10.1029/2008GL033256

Wathelet M, Jongmans D, Ohrnberger M (2004) Surface-wave inversion using a direct search algorithm and its application to ambient vibration measurements. Near Surf Geophys 2:211–221. https://doi.org/10.3997/1873-0604.2004018

Widiyantoro S, Van Der Hilst R (1996) Structure and evolution of lithospheric slab beneath the Sunda arc, Indonesia. Science (80-) 271:1566–1570. https://doi.org/10.1126/science.271.5255.1566

Widiyantoro S, Pesicek JD, Thurber CH (2011) Subducting slab structure below the eastern Sunda arc inferred from non-linear seismic tomographic imaging. Geol Soc Spec Publ 355:139–155. https://doi.org/10.1144/SP355.7

Widiyantoro S, Gunawan E, Muhari A et al (2020) Implications for megathrust earthquakes and tsunamis from seismic gaps south of Java Indonesia. Sci Rep. https://doi.org/10.1038/s41598-020-72142-z

Yao H, van Der Hilst RD, de Hoop MV (2006) Surface-wave array tomography in SE Tibet from ambient seismic noise and two-station analysis—I. Phase Velocity Maps. Geophys J Int 166:732–744. https://doi.org/10.1111/j.1365-246X.2006.03028.x

Zulfakriza Z, Saygin E, Cummins PR et al (2014) Upper crustal structure of central Java, Indonesia, from transdimensional seismic ambient noise tomography. Geophys J Int 197:630–635. https://doi.org/10.1093/gji/ggu016

Zulfakriza Z, Nugraha AD, Widiyantoro S et al (2020) Tomographic imaging of the Agung-Batur Volcano Complex, Bali, Indonesia, from the ambient seismic noise field. Front Earth Sci 8:1–11. https://doi.org/10.3389/feart.2020.00043

Publisher's Note

Springer Nature remains neutral with regard to jurisdictional claims in published maps and institutional affiliations.